

Phonon anomalies associated with spin reorientation in the Kagome ferromagnet Fe_3Sn_2

Ge He Leander Peis Ramona Stumberger Lilian Prodan Vladimir Tsurkan Nico Unglert
Livia Chioncel István Kézsmárki Rudi Hackl

Dr. Ge He, Leander Peis

Walther Meissner Institut, Bayerische Akademie der Wissenschaften, 85748 Garching, Germany

Nico Unglert, Prof. Dr. Livia Chioncel

Theoretische Physik III, Institut für Physik, Universität Augsburg, Universitätsstrasse 1 (Physik Süd),
86159 Augsburg, Germany

Dr. Lilian Prodan, Dr. Vladimir Tsurkan, Prof. Dr. István Kézsmárki

Experimentalphysik V, Institut für Physik, Universität Augsburg, Universitätsstrasse 1 (Physik Süd),
86159 Augsburg, Germany

Ramona Stumberger, Prof. Dr. Rudi Hackl

Technische Universität München, Fakultät für Physik, 85748 Garching, Germany

Walther Meissner Institut, Bayerische Akademie der Wissenschaften, 85748 Garching, Germany

Email Address: hackl@tum.de

Keywords: *Phonons, light scattering, magnetism*

Polarization- and temperature-dependent Raman data along with theoretical simulations are presented for the Kagome ferromagnet Fe_3Sn_2 . Eight out of nine expected phonon modes were identified. The experimental energies compare well with those from the simulations. The analysis of the line widths indicates relatively strong phonon-phonon coupling in the range 0.1 to 1. The temperature-dependent frequencies of three A_{1g} modes show weak anomalies at approximately 100 K. In contrast, the linewidths of all phonon modes follow the conventional exponential broadening up to room temperature except for the softest A_{1g} mode, whose width exhibits a kink close to 100 K and becomes nearly constant for $T > 100$ K. These features are indicative of a spin reorientation taking place in the temperature range above 100 K which might arise from spin-phonon coupling. The low-energy part of the electronic continuum in E_g symmetry depends strongly on temperature. The possible reasons include particle-hole excitation tracking the resistivity, a spin-dependent gap or spin fluctuations.

1 Introduction

Materials with novel properties and functionalities have intriguing scientific and applied perspectives. In particular magnets with exotic ground states continue to attract attention since the properties may be tailored *via* the lattice and/or the electronic band structure. Fe_3Sn_2 is a layered Kagome ferromagnet with a very high Curie temperature $T_C = 670$ K. The Fe-Sn bi-layers are separated by Sn mono-layers [1, 2, 3, 4] as shown in Fig. 1(a). Due to its out-of-plane anisotropy [2, 3] with the magnetic easy axis perpendicular to the Kagome layers, magnetic stripes and a variety of magnetic bubbles have been observed in thin lamellae using Lorentz transmission electron microscopy [5, 6, 7, 8]. Since the material possesses inversion symmetry, these mesoscale magnetic textures do not form due to the antisymmetric part of the exchange coupling tensor, i.e. the Dzyaloshinskii-Moriya interaction, but due to a competition between the out-of-plane anisotropy and the magnetic dipole-dipole interaction. The magnetic anisotropy of the system is also linked to the reconstruction of its band structure in a magnetic field: A strong shift of bands close to the Fermi energy was found to be dependent not only on the magnitude but also on the orientation of the magnetic field [9]. Moreover, indications of a temperature-driven spin reorientation, from out-of-plane at high temperatures towards in-plane at low temperatures, have been found earlier in Mössbauer [2, 3], x-ray [4] and transport studies [10]. Optical absorption experiments [11] reveal an additional feature in the 10 meV range below 150 K and associate it with this spin reorientation. Similarly, transport and magnetisation experiments [performed on our own samples and plotted in Fig. 1(b) and (c)] show a cross-over temperature close to 100 K and will be discussed in detail in section 2.1.

There are various other effects in a planar hexagonal lattice such as massless Dirac fermions. As opposed to graphene the tips of the cones typically intersect below the Fermi energy E_F and may become massive in the presence of spin-orbit coupling (SOC) [9, 12]. Recently, the existence of flat bands at approximately 200 meV below E_F in confined regions of the Brillouin zone was associated with magnetic ordering in Fe_3Sn_2 [13]. These observations and suggestions are among the main motivations for the present work, focusing on spin reorientation and band reconstruction phenomena in Fe_3Sn_2 and its consequences for the lattice dynamics and charge response, both probed by Raman spectroscopy.

Spin textures usually entail a huge anomalous Hall effect (AHE) being associated with the Berry phase the electrons pick up upon moving across a magnetic background [14]. Thus Fe_3Sn_2 has similarities with, e.g., MnSi [15] and various other compounds. The origin, however, of the rather complex itinerant ferromagnetism with a high T_C and a spin reorientation at some 100 K is elusive. The most popular approaches are based on the Hubbard model and either favor flat-band ferromagnetism [16, 17, 18] or a trade-off between potential and kinetic energy [13, 19, 20]. The latter case is reminiscent of the magnetism in $\text{Fe}(\text{Se}, \text{Te})$ where itinerant and nearly localized spins seem to cooperate as well [21, 22, 23].

It is unlikely that the magnetism in Fe_3Sn_2 can be observed directly in a similar fashion as in FeSe since the two-magnon excitations typical for antiferromagnets [24] do not exist here. However, indirect signatures of spin order, the spin reorientation or the interaction between spin, lattice and electrons may be expected, in particular gaps between flatbands such as in the optical experiments [11] or phonon renormalization effects as in MnSi [25]. In this, to our knowledge first, Raman study of the topological material Fe_3Sn_2 we start with analyzing the phonons.

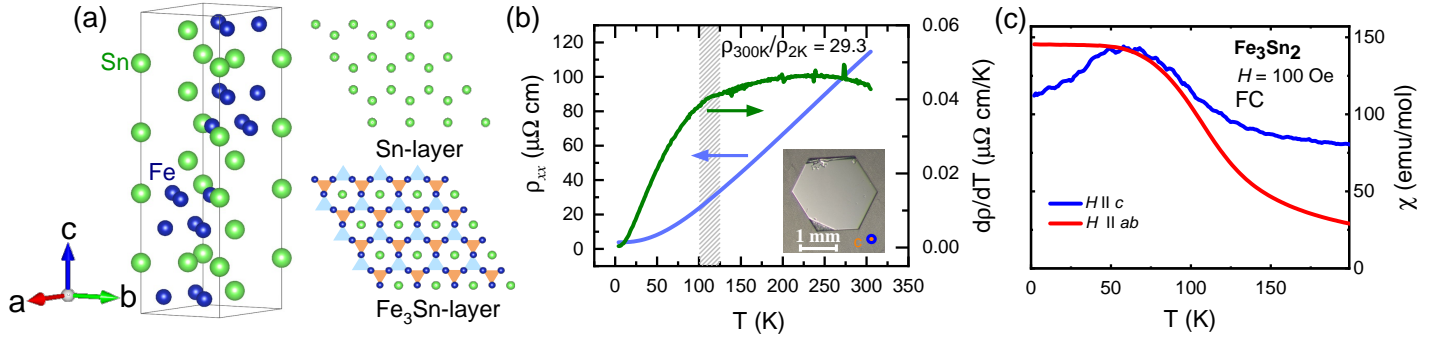


Figure 1: Properties of Fe_3Sn_2 . (a) Crystal structure (left). The crystals consist of hexagonal Sn-layers sandwiched between Kagome Fe_3Sn double layers (right). (b) Resistivity $\rho(T)$ of Fe_3Sn_2 . $\rho(T)$ (blue) was measured on a crystal from the same batch as the sample used here. $d\rho(T)/dT$ (green, right axis) is nearly constant above 100 K indicating a linear temperature dependence of $\rho(T)$. Below a rather well-defined kink at 100 K the slope changes rapidly. (c) Anisotropic susceptibility $\chi_i(T)$ for field orientations as indicated. The sample was cooled in an applied field of $\mu_0 H = 0.01$ T. $\chi_{ab}(T)$ increases monotonously and almost saturates below 50 K. $\chi_c(T)$ has a maximum between 50 and 100 K.

2 Experimental Methods

2.1 Samples

Fe_3Sn_2 single crystals have been grown by the chemical transport reaction method. As starting material we used pre-synthesized poly-crystalline powder prepared by solid state reaction from the high-purity elements Fe (99.99 %) and Sn (99.995 %). Iodine was used as the transport agent. The growth was performed in SiO_2 ampoules in two-zone furnaces at temperatures between 730 and 680 K. After 4-6 weeks of transport, the single-crystals, having a plate-like form with a thickness in the range 20-40 μm along the c -axis and 3-5 mm in the ab -plane [see inset of Fig.1(b)], were found in the hot part of ampoule.

The sample used for the experiments has a Residual Resistance Ratio of $RRR = 29.3$ [Fig.1(b)] indicating high crystalline quality. The derivative of the resistivity, $d\rho(T)/dT$ (green graph), indicates a qualitative change of the slope at approximately 100 K where all spins are expected to be finally parallel to the ab -plane. Fig. 1(c) shows the temperature dependences of the in-plane and out-of-plane magnetic

susceptibilities, χ_{ab} and χ_c , respectively. For the analysis of the out-of-plane susceptibility, demagnetization effects had to be taken into account because of the thin-slab geometry of the sample. At high temperatures, χ_c is more than three times larger than χ_{ab} . Toward 100 K this difference diminishes. Below 100 K χ_c starts to decrease while χ_{ab} saturates. Consequently, at low temperatures the c -axis becomes harder than the in-plane direction with $\chi_{ab}/\chi_c \approx 1.2$ at 2 K. In the same temperature range, where χ_{ab} and χ_c cross each other, the resistivity shows a kink, as best seen in its temperature derivative in Fig. 1(b). After witnessing the spin reorientation in magnetic and transport properties, we turn to the Raman spectroscopic study of Fe_3Sn_2 , the main subject of this work.

2.2 Light scattering

We performed polarized inelastic light scattering experiments at an excitation wavelength of 575 nm (Coherent GENESIS MX-SLM577-500). The samples were attached to the cold finger of a ^4He flow cryostat. Polarized photons hit the sample at an angle of incidence of 66° yielding a spot size of approximately $50 \times 100 \mu\text{m}^2$. The polarized scattered photons were collected along the surface normal of the sample and focused on the entrance slit of a double monochromator. The resolution of the spectrometer is set at 2.8 cm^{-1} . Polarized photons having the selected energy were recorded with a CCD detector. The number of photons per second is proportional to the Van-Hove function $S(q \approx 0, \Omega) = \hbar/\pi \{1 + n(\Omega, T)\} \chi''(\Omega, T)$ where $n(\Omega, T)$ is the Bose factor and χ'' is the imaginary part of Raman response function.

For the measurements shown here we used only two polarization configurations, RR and RL , where $R = 2^{-1/2}(x + iy)$ and $L = 2^{-1/2}(x - iy)$ for the incoming light (first symbol) inside the sample. An absorbed laser power of $P_{\text{abs}} = 4.0 \text{ mW}$ independent of the polarization is used. P_{abs} induced a heating in the spot region of approximately 1-2 K/mW. Here only the holder temperature is indicated. Since we use (near) backscattering configurations both signs change for the scattered light (second symbol). The details of the Raman selection rules will be discussed below. Due to the symmetric shape of the observed phonon modes and the narrow line width (FWHM), $\Gamma_L(T) \ll \omega_0(T)$, where ω_0 is the resonance energy of the respective mode, their line shapes may be described by temperature-dependent Lorentz functions.

2.3 Selection rules and simulations

The Raman-active phonon energies and eigenvectors at the Γ point of the Brillouin zone were derived on the basis of the crystal structure using density functional theory (DFT). The symmetry selection rules may be determined from the point group and the atomic positions in the crystal. The space group of Fe_3Sn_2 is $R\bar{3}m$ (No. 166) and belongs to D_{3d} ($\bar{3}1m$) point group. The corresponding Raman tensors read

$$A_{1g} = \begin{pmatrix} a & 0 & 0 \\ 0 & a & 0 \\ 0 & 0 & b \end{pmatrix}, \quad (1)$$

$$E_g^{(1)} = \begin{pmatrix} c & 0 & 0 \\ 0 & -c & d \\ 0 & d & 0 \end{pmatrix}, \quad \text{and} \quad (2)$$

$$E_g^{(2)} = \begin{pmatrix} 0 & -c & -d \\ -c & 0 & 0 \\ -d & 0 & 0 \end{pmatrix}. \quad (3)$$

According to the Wyckoff positions of the Fe ($18h$) and Sn atoms ($6c$) in Fe_3Sn_2 , there are 4 A_{1g} and 5 E_g Raman-active phonons. On the basis of the Raman tensors [Eqs. (1), (2), and (3)] the A_{1g} and E_g phonons, may be projected separately in the RR and RL channel, respectively.

Electronic structure calculations were carried out using DFT and the projector augmented wave (PAW) method as implemented in VASP [26, 27, 28, 29]. The generalized gradient approximation as parameterized in the Perdew-Burke-Ernzerhof (PBE) functional [30] was used to treat exchange and correlation effects. The cutoff for the plane-wave basis was chosen as 680 eV, and the Brillouin-zone was sampled

Table 1: Phonon energies and widths (FWHM) of Fe_3Sn_2 at 4.2 K. Fe_3Sn_2 has four fully symmetric and five E_g phonon modes four of which were observed experimentally. In addition to the theoretical and experimental energies ω_0 and Lorentzian widths $\Gamma_L(T)$ the table displays also the phonon-phonon coupling parameters $\lambda_{i,\text{ph-ph}}$ as derived from the approximative harmonic fits to the temperature dependent line widths. The two values of $\lambda_{1,\text{ph-ph}}$ for $A_{1g}(1)$ correspond to temperatures below and above 100 K as indicated in Fig. 3(a) by dashed-dotted and dotted lines, respectively.

Phonon		$A_{1g}(1)$	$A_{1g}(2)$	$A_{1g}(3)$	$A_{1g}(4)$	$E_g(1)$	$E_g(2)$	$E_g(3)$	$E_g(4)$	$E_g(5)$
Energy (cm^{-1})	Simulation	83.9	140.1	232.1	241.8	92.7	138.2	147.1	196.7	278.3
	Experiment	86.6	146.8	237.7	251.6	94.3	133.8	147.0	199.8	-
FWHM (cm^{-1})		4.5	4.1	4.7	4.9	3.6	3.1	3.8	4.1	-
$\lambda_{i,\text{ph-ph}}$		0.20; 0.05	0.14	0.68	0.74	0.11	1.11	0.29	0.42	-

with a $10 \times 10 \times 10$ Γ -centered Monkhorst-Pack grid. The Fe_3Sn_2 crystal structure reported in [4] was fully relaxed until the forces on all atoms were below $0.001 \text{ eV} \cdot \text{\AA}^{-1}$. Γ -point phonon calculations were performed using Density Functional Perturbation theory as implemented in VASP. For the symmetry analysis of all phonon modes the PHONOPY package [31] was employed, allowing for an unambiguous assignment to the experimental frequencies, as compiled in Table 1. The eigenvectors characterizing the atomic displacement coordinates are listed in Supplementary Materials A.

3 Results and Discussions

The main focus of the paper is placed on the analysis of the phonon modes in the temperature range of the re-orientation of the Fe spins. Briefly, we will also discuss the electronic continuum.

3.1 Phonons

Figures 2(a) and (b) show, respectively, the A_{1g} and E_g Raman spectra at temperatures ranging from 4.2 K to 320 K. We can identify four A_{1g} phonons and four out of the expected five E_g phonons. These phonons harden continuously with decreasing temperature. The absent fifth E_g phonon might be too weak in intensity to be detected.

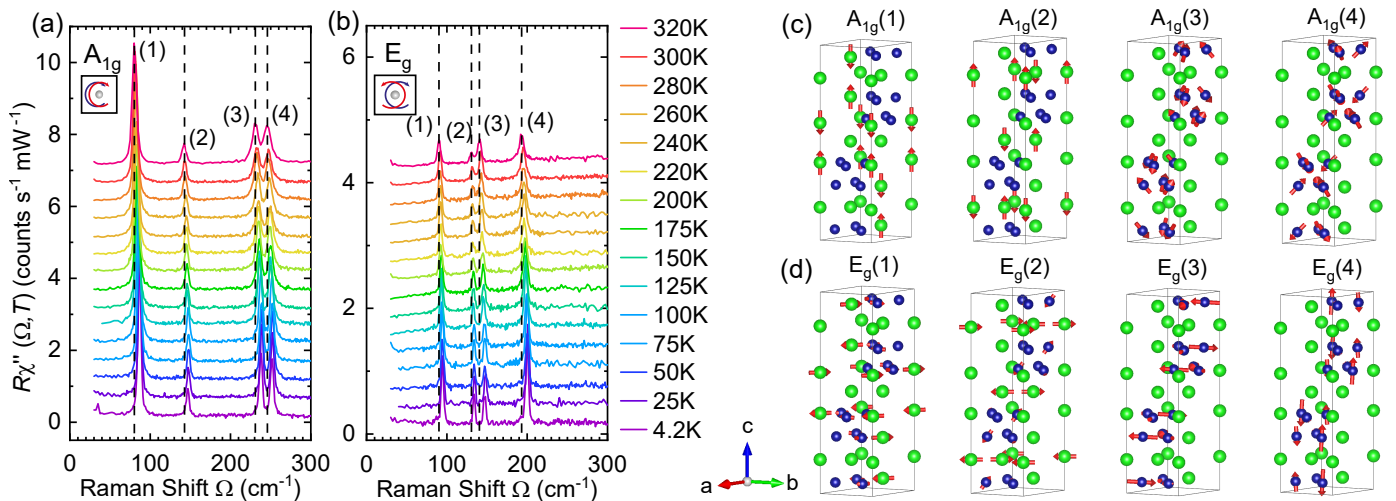


Figure 2: Raman spectra and phonon eigenvectors of Fe_3Sn_2 . (a) and (b) Temperature dependence of the eight observed phonon modes in Fe_3Sn_2 . The spectra at the lowest temperature have the experimental intensity. The A_{1g} spectra are consecutively offset by 0.5 cts/(s mW) and those in E_g symmetry by 0.3 cts/(s mW) each for clarity. The clockwise and counter-clockwise half circle arrows indicate the R and L polarization in (a) and (b), respectively. Columns (a) and (b) separately display the A_{1g} - and E_g phonon modes, respectively, (c) and (d) show the respective eigenvectors (small amplitudes omitted).

For a quantitative analysis the phonon peaks were fitted using a Voigt function, which is a convolution of the Lorentzian shape of the phonons and a Gaussian for the spectral resolution of the setup. In the narrow spectral range displayed in Fig. 2 and the laser line used, the resolution is constant and was set at 2.8 cm^{-1} . Thus the widths indicated, directly correspond to those of the phonons. The reasonable quality of the fits (see Fig. S1) indicates that the Lorentzian widths $\Gamma_L(T)$ result from the finite life time of the phonons, determined by phonon-phonon decay into two modes having the same energy $\omega_0/2$ and opposite wave vectors \mathbf{k} and $-\mathbf{k}$ [32].

The peak energies and linewidths (FWHM) derived in this way are depicted in Fig. 3 and 4, and labeled consecutively from low to high. Their respective values at 4.2 K are listed in Table 1 and found to be in good agreement with the simulation. All phonon modes become harder and narrower upon cooling. The usual changes in width and energy are related to the unharmonic decay [32] and the lattice contraction [33]. However, as opposed to the E_g modes some of the A_{1g} modes show weak but significant deviations from the expected behavior in the temperature range around 100 K. In particular, kinks are observed in the energies of modes 1, 3, and 4 [see hatched range in Fig. 3(a) and (c)]. After remeasuring the A_{1g} spectra [open symbols in Fig. 3(a)–(d)] the kinks can still be observed but are shifted slightly. The origin of this shift is not entirely clear but may be related to the first-order nature of the reorientation transition and the then expected hysteresis [34]. In fact, the open points were obtained upon heating from low to high temperature in an uninterrupted series whereas the black points were measured upon cooling as indicated in the figure caption. More experiments are required to finally clarify this issue.

The conventional reduction of the phonon widths with decreasing temperature can be understood in terms of the anharmonic decay described above [32] and may be represented by

$$\Gamma_L(T) = \Gamma_{L,0} \left(1 + \frac{2\lambda_{\text{ph-ph}}}{\exp(\frac{\hbar\omega_0}{2k_B T}) - 1} \right). \quad (4)$$

$\Gamma_{L,0}(T)$ and ω_0 in Eq. (4) can be extrapolated to zero from the experimental points below 50 K, leaving only the phonon-phonon coupling $\lambda_{i,\text{ph-ph}}$ as a free parameter. The corresponding curves are indicated in red in Fig. 3 and 4, and the resulting values for $\lambda_{\text{ph-ph}}$ are compiled in Table 1. As opposed to the linewidth the phonon energy depends on the occupation and the thermal expansion where the latter one is approximately larger by two orders of magnitude and depends crucially on the variation of the interatomic potential with distance [33]. The temperature dependences of the phonon width and energy are related by the usual Kramers-Kronig transformation and were determined for constant volume by Balkanski and coworkers [35]. However, in an experiment the pressure rather than the volume are constant, and this approach is not applicable (see, e.g., Ref. [25]). Thus, the analysis of the phonon energy requires the knowledge of the thermal expansion and the Grüneisen parameters which are currently not available.

All phonons except for one show essentially conventional behavior and become exponentially narrower upon cooling. Only the $A_{1g}(1)$ phonon at 86 cm^{-1} shows unexpected behavior directly in the data, and the description of the temperature dependence according to Eq. (4) is similar to the other modes only for $T \leq 100 \text{ K}$ [dashed-dotted in Fig. 3(a)] and yields $\lambda_{1,\text{ph-ph}} = 0.2$. For $T \geq 100 \text{ K}$ (dotted) the width is almost temperature independent corresponding to an unusually small coupling of $\lambda_{1,\text{ph-ph}} = 0.05$. So we conclude that the symmetric phonon-phonon decay channel is essentially blocked when the spins point along the c -axis and becomes accessible only when the spins are rotated into the ab -plane. This hand-waving argument certainly needs further theoretical analysis but a realistic model of the spin-phonon coupling is beyond the scope of this paper and requires complex, presumably numerical work.

3.2 E_g continuum at low energy

Since Fe_3Sn_2 is purely metallic and orders at $T_C \approx 670 \text{ K}$, gaps or isolated electronic or magnetic modes are not immediately expected in the temperature range studied. Due to the magnetic anisotropy one may expect to see a single magnon at finite energy given by the anisotropy field. However, our microwave

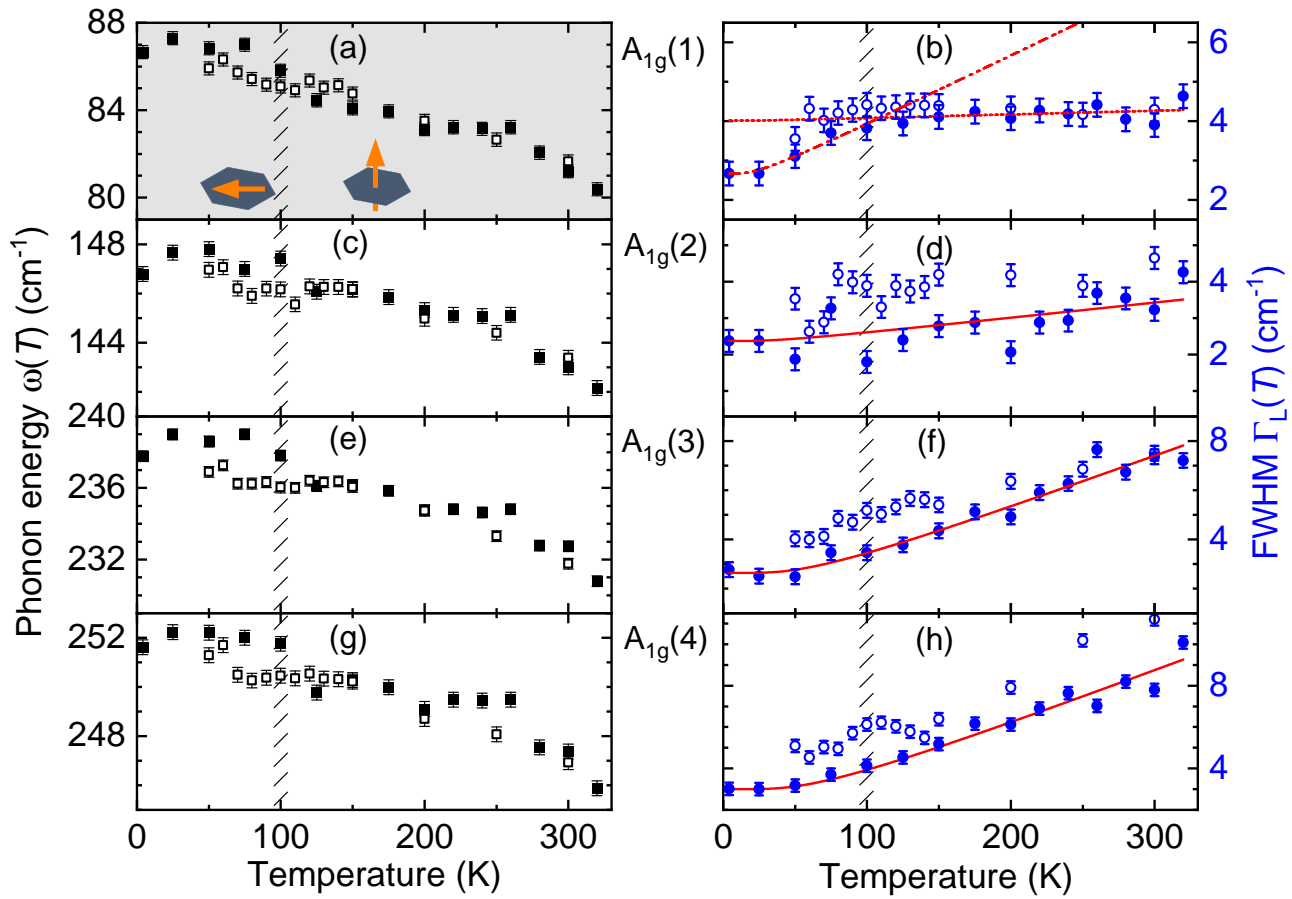


Figure 3: Phonon energies ω_0 (black) and Lorentzian widths Γ_L (blue) of Fe_3Sn_2 in A_{1g} symmetry. The average magnetization with respect to the ab -plane is indicated in (a). The parameters are derived by fitting procedures as described in the text. The first series of measurements (full black and blue symbols) was taken at temperatures listed in the following sequence: [320, 300, 200, 100, 75, 50, 25, 4.2, 125, 150, 175, 220, 240, 260, 280] K. The second series (open black and blue symbols) was measured in a row warming up from 50 K with a distance of 10 K in the interesting range. All linewidths Γ_L were fitted according to equation (4) (red lines). The linewidth of the A_{1g} -mode at 86 cm^{-1} in (a) shows anomalous behavior, displaying a change in the expected temperature dependence at approximately 100 K as indicated by the hatched area. Eq. (4) yields $\lambda_{1,\text{ph-ph}} = 0.2$ at low temperature and only 0.05 above 100 K.

experiments show that the energy is presumably too small for the Raman experiment. In addition, fluctuations as a consequence of geometric frustration may smear out the energies.

The small variations with temperature of the E_g spectra below 100 cm^{-1} , as shown in Fig. 5, look unspectacular at first glance. However, the increase at low temperature must be considered real since a peak at approximately 47 cm^{-1} can be resolved at 4.2 K rather than a divergence towards zero energy as in the case of diffuse scattering of the laser light. The intensity increase may either originate from particle-hole excitations reflecting the temperature dependence of the resistivity [see Fig. 1(b)] or from interband transitions as suggested by the optical conductivity [11] or from fluctuations similar to FeSe [24]. For clarification larger crystals with flat surfaces are necessary.

Compared with the E_g spectra, the A_{1g} continuum is essentially temperature-independent (see Supplementary Materials C). As in the case of the E_g spectra, the data are reliable above 30 cm^{-1} . Obviously, different excitations or regions of the Brillouin zone are projected in the two symmetries. Given the correspondence between transport and low-energy E_g spectra, the most likely explanation is that the carrier relaxation observed in the A_{1g} spectra is almost temperature independent. This interesting anisotropy calls for more studies in optimized samples.

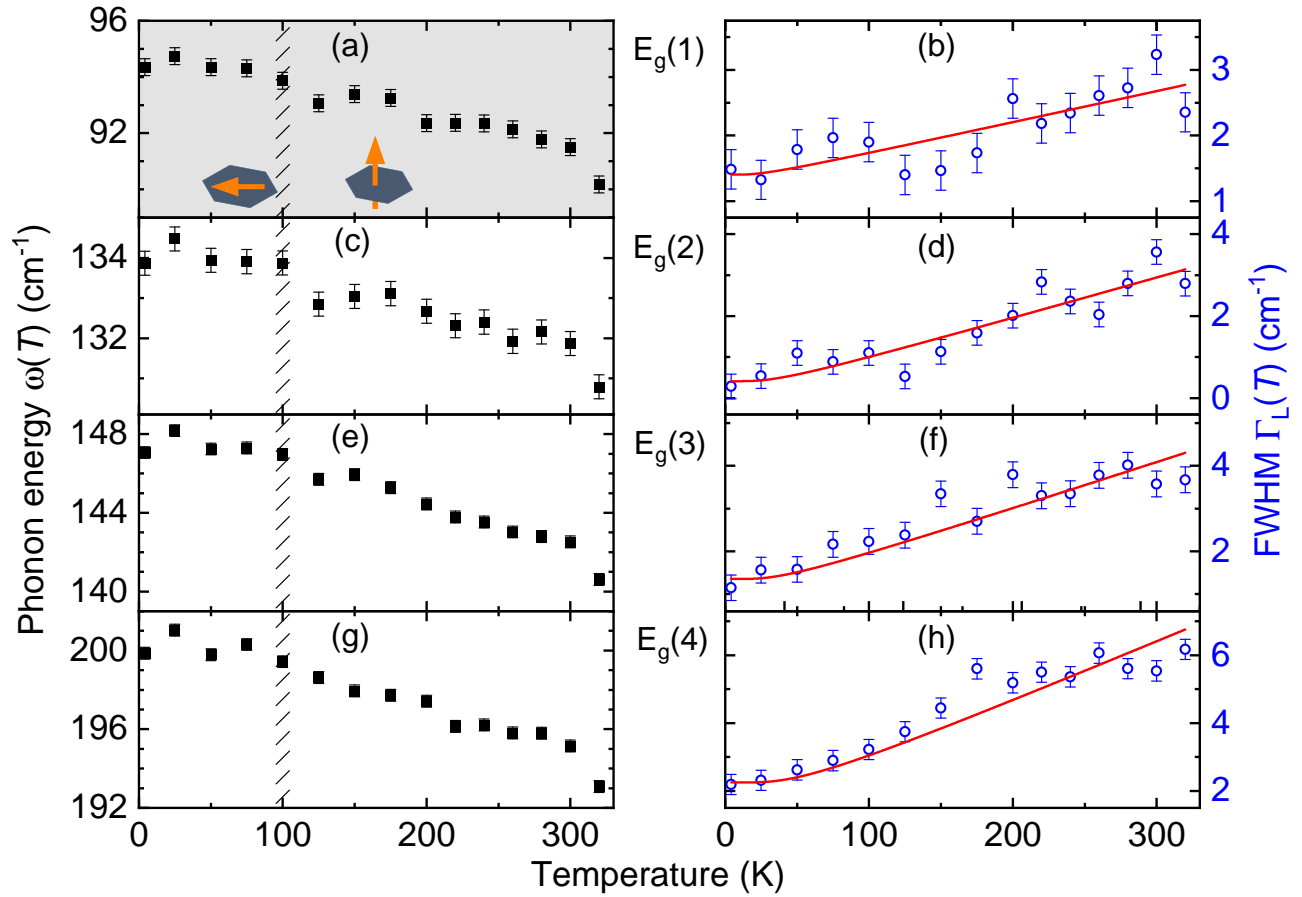


Figure 4: Phonon energies ω_0 (black) and Lorentzian widths Γ_L (blue) of Fe_3Sn_2 in E_g symmetry. The linewidths and phonon energies behave like usual phonons without anomaly near the spin reorientation transition temperature.

4 Conclusions

We have studied the Kagome ferromagnet Fe_3Sn_2 using polarized Raman scattering. We identified all but one phonon lines and compared them to simulations of the lattice dynamics on the basis of density functional theory. The agreement between predicted and experimental phonon energies is better than 5 % for all lines. All phonons broaden upon heating. By assuming symmetric decay of the lines at ω_0 and $|\mathbf{q}| \approx 0$ into two lines at $\omega_0/2$ and $\pm\mathbf{k}$ the dimensionless phonon-phonon coupling $\lambda_{i,\text{ph-ph}}$ was extracted and found to be in the range 0.1 to 1.1 for all lines and temperatures with one exception: The A_{1g} phonon with the lowest energy exhibits $\lambda_{1,\text{ph-ph}} = 0.2$ below 100 K and $\lambda_{1,\text{ph-ph}} = 0.05$ above 100 K thus it has only very small phonon-phonon coupling at temperatures with the spins aligned along the c -axis parallel to the motion of the Sn atoms for the $A_{1g}(1)$ mode. For this specific eigenvector the coupling to the Fe spins parallel to the c -axis is certainly small, and one may speculate that the relatively large $\lambda_{i,\text{ph-ph}}$ values of the other phonons result from coupling *via* the spins. As soon as the spins rotate into the plane also the $A_{1g}(1)$ mode couples to the spins and thus participates in the anharmonic decay.

Because of the relatively high Curie temperature of $T_C = 670$ K in Fe_3Sn_2 one does not expect strong changes in the electronic properties below room temperature. Yet, the E_g continuum exhibits a substantial variation with temperature at low energies which are reminiscent of the strong temperature dependence of the resistivity $\rho(T)$. However, the low-energy peak in the E_g spectra may also originate from a band gap induced by the spin reorientation as suggested by optical measurements [11], although the rather different energies in the two experiments argues against this possibility, or from magnetic fluctuations in a geometrically frustrated system. There are no indications of a flat band in the 200 meV range. Yet, with the available equipment we cannot obtain a sufficiently high data quality for a quantitative analysis.

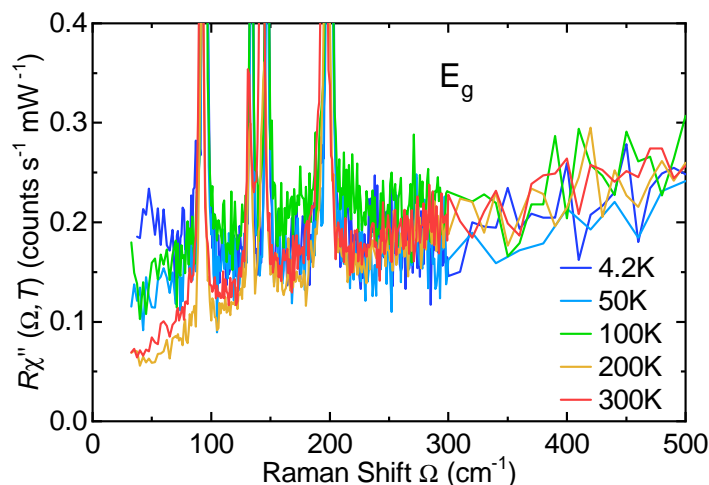


Figure 5: Electronic continuum in E_g symmetry at temperatures as indicated. The factor R is a constant of proportionality which absorbs all experimental factors. The contribution from the laser line is negligible above 30 cm^{-1} . The intensity below 150 cm^{-1} increases continuously upon cooling which implies a concomitant increase of the initial slope indicating a metallic ground state in agreement with the transport result. The increase at the limit $\Omega \rightarrow 0$ is a real effect since the spectra at 4.2 K have a peak at finite energy and then decrease again as opposed to a laser-induced divergence.

Acknowledgements

We thank Y.-F. Xu for fruitful discussions. This work is supported by the Deutsche Forschungsgemeinschaft (DFG) through the coordinated programme TRR80 (Project-ID 107745057) and project HA 2071/12-1. G. He would like to thank the Alexander von Humboldt Foundation for support through a fellowship.

Author contributions

G. He and L. Peis contributed equally to the Raman study.

References

- [1] G. Trumphy, E. Both, C. Djéga-Mariadassou, P. Lecocq, *Phys. Rev. B* **1970**, *2* 3477.
- [2] G. Le Caër, B. Malaman, B. Roques, *J. Phys. F: Met. Phys.* **1978**, *8* 323.
- [3] B. Malaman, C. Fruchart, G. Le Caër, *J. Phys. F: Met. Phys.* **1978**, *8* 2389.
- [4] L. A. Fenner, A. A. Dee, A. S. Wills, *J. Phys. Condens. Matter* **2009**, *21* 452202.
- [5] Z. Hou, W. Ren, B. Ding, G. Xu, Y. Wang, B. Yang, Q. Zhang, Y. Zhang, E. Liu, F. Xu, W. Wang, G. Wu, X. Zhang, B. Shen, Z. Zhang, *Adv. Mater.* **2017**, *29* 1701144.
- [6] Z. Hou, Q. Zhang, G. Xu, C. Gong, B. Ding, Y. Wang, H. Li, E. Liu, F. Xu, H. Zhang, Y. Yao, G. Wu, X.-x. Zhang, W. Wang, *Nano Lett.* **2018**, *18* 1274.
- [7] J. Tang, Y. Wu, L. Kong, W. Wang, Y. Chen, Y. Wang, Y. Soh, Y. Xiong, M. Tian, H. Du, *Natl. Sci. Rev.* **2020**, *8* nwaa200.
- [8] J. Tang, L. Kong, Y. Wu, W. Wang, Y. Chen, Y. Wang, J. Li, Y. Soh, Y. Xiong, M. Tian, H. Du, *ACS Nano* **2020**, *14* 10986.
- [9] J.-X. Yin, S. S. Zhang, H. Li, K. Jiang, G. Chang, B. Zhang, B. Lian, C. Xiang, I. Belopolski, H. Zheng, T. A. Cochran, S.-Y. Xu, G. Bian, K. Liu, T.-R. Chang, H. Lin, Z.-Y. Lu, Z. Wang, S. Jia, W. Wang, M. Z. Hasan, *Nature* **2018**, *562* 91.
- [10] Q. Wang, S. Sun, X. Zhang, F. Pang, H. Lei, *Phys. Rev. B* **2016**, *94* 075135.

- [11] A. Biswas, O. Iakutkina, Q. Wang, H. C. Lei, M. Dressel, E. Uykur, *Phys. Rev. Lett.* **2020**, *125* 076403.
- [12] Z.-Z. Lin, X. Chen, *phys. stat. solidi (RRL) Rapid Research Letters* **2020**, *14* 1900705.
- [13] Z. Lin, J.-H. Choi, Q. Zhang, W. Qin, S. Yi, P. Wang, L. Li, Y. Wang, H. Zhang, Z. Sun, L. Wei, S. Zhang, T. Guo, Q. Lu, J.-H. Cho, C. Zeng, Z. Zhang, *Phys. Rev. Lett.* **2018**, *121* 096401.
- [14] N. Nagaosa, J. Sinova, S. Onoda, A. H. MacDonald, N. P. Ong, *Rev. Mod. Phys.* **2010**, *82* 1539.
- [15] C. Franz, F. Freimuth, A. Bauer, R. Ritz, C. Schnarr, C. Duvinage, T. Adams, S. Blügel, A. Rosch, Y. Mokrousov, C. Pfleiderer, *Phys. Rev. Lett.* **2014**, *112* 186601.
- [16] A. Mielke, *J. Phys. A* **1991**, *24* 3311.
- [17] A. Mielke, *J. Phys. A* **1991**, *24* L73.
- [18] A. Mielke, *J. Phys. A* **1992**, *25* 4335.
- [19] Y. Nagaoka, *Phys. Rev.* **1966**, *147* 392.
- [20] F. Pollmann, P. Fulde, K. Shtengel, *Phys. Rev. Lett.* **2008**, *100* 136404.
- [21] Z. P. Yin, K. Haule, G. Kotliar, *Nature Mater.* **2011**, *10* 932.
- [22] I. Leonov, S. L. Skornyakov, V. I. Anisimov, D. Vollhardt, *Phys. Rev. Lett.* **2015**, *115* 106402.
- [23] K. M. Stadler, Z. P. Yin, J. von Delft, G. Kotliar, A. Weichselbaum, *Phys. Rev. Lett.* **2015**, *115* 136401.
- [24] A. Baum, H. N. Ruiz, N. Lazarević, Y. Wang, T. Böhm, R. Hosseinian Ahangharnejhad, P. Adelman, T. Wolf, Z. V. Popović, B. Moritz, T. P. Devereaux, R. Hackl, *Commun. Phys.* **2019**, *2* 14.
- [25] H.-M. Eiter, P. Jaschke, R. Hackl, A. Bauer, M. Gangl, C. Pfleiderer, *Phys. Rev. B* **2014**, *90* 024411.
- [26] G. Kresse, J. Hafner, *Phys. Rev. B* **1994**, *49* 14251.
- [27] G. Kresse, J. Furthmüller, *Comput. Mater. Sci.* **1996**, *6* 15.
- [28] G. Kresse, J. Furthmüller, *Phys. Rev. B* **1996**, *54* 11169.
- [29] G. Kresse, D. Joubert, *Phys. Rev. B* **1999**, *59* 1758.
- [30] J. P. Perdew, K. Burke, M. Ernzerhof, *Phys. Rev. Lett.* **1996**, *77* 3865.
- [31] A. Togo, I. Tanaka, *Scr. Mater.* **2015**, *108* 1.
- [32] P. G. Klemens, *Phys. Rev.* **1966**, *148* 845.
- [33] C. Postmus, J. R. Ferraro, S. S. Mitra, *Phys. Rev.* **1968**, *174* 983.
- [34] N. Kumar, Y. Soh, Y. Wang, Y. Xiong, *Phys. Rev. B* **2019**, *100* 214420.
- [35] M. Balkanski, R. F. Wallis, E. Haro, *Phys. Rev. B* **1983**, *28* 1928.